CARDIAC SIDE EFFECTS

Visnagin protects against doxorubicin-induced cardiomyopathy through modulation of mitochondrial malate dehydrogenase

Yan Liu,[1,2]* Aarti Asnani,[1,2]* Lin Zou,[3] Victoria L. Bentley,[4] Min Yu,[5] You Wang,[1,2]
Graham Dellaire,[4,6] Kumar S. Sarkar,[1,2] Matthew Dai,[1] Howard H. Chen,[1,7] David E. Sosnovik,[1,7]
Jordan T. Shin,[1] Daniel A. Haber,[5,8] Jason N. Berman,[9,10] Wei Chao,[3] Randall T. Peterson[1,2]†

Doxorubicin is a highly effective anticancer chemotherapy agent, but its use is limited by its cardiotoxicity. To develop a drug that prevents this toxicity, we established a doxorubicin-induced cardiomyopathy model in zebrafish that recapitulates the cardiomyocyte apoptosis and contractility decline observed in patients. Using this model, we screened 3000 compounds and found that visnagin (VIS) and diphenylurea (DPU) rescue the cardiac performance and circulatory defects caused by doxorubicin in zebrafish. VIS and DPU reduced doxorubicin-induced apoptosis in cultured cardiomyocytes and in vivo in zebrafish and mouse hearts. VIS treatment improved cardiac contractility in doxorubicin-treated mice. Further, VIS and DPU did not reduce the chemotherapeutic efficacy of doxorubicin in several cultured tumor lines or in zebrafish and mouse xenograft models. Using affinity chromatography, we found that VIS binds to mitochondrial malate dehydrogenase (MDH2), a key enzyme in the tricarboxylic acid cycle. As with VIS, treatment with the MDH2 inhibitors mebendazole, thyroxine, and iodine prevented doxorubicin cardiotoxicity, as did treatment with malate itself, suggesting that modulation of MDH2 activity is responsible for VIS' cardioprotective effects. Thus, VIS and DPU are potent cardioprotective compounds, and MDH2 is a previously undescribed, druggable target for doxorubicin-induced cardiomyopathy.

INTRODUCTION

Doxorubicin is a potent chemotherapy drug widely used against a broad range of cancers including solid tumors and leukemia. Like other members of the anthracycline class, its usage is greatly limited by the risk of severe cardiotoxicity, and cumulative dosages greater than 300 mg/m^2 exponentially increase the risk of heart failure (1). Nevertheless, even at lower doses, some patients inevitably develop heart disease many years after therapy (2). Therefore, adjuvant therapies that protect the heart but do not interfere with tumor treatment are needed. Such drugs could benefit cancer patients by preventing cardiomyopathy and by permitting the use of more effective anthracycline dosages.

The underlying mechanisms of anthracycline cardiotoxicity have not been fully elucidated. A plethora of proapoptotic effects such as DNA damage, lipid peroxidation, reactive oxygen species (ROS) overproduction, calcium mishandling, ATP (adenosine 5′-triphosphate) depletion, contractile protein degradation, and transcription misregulation have all been associated with anthracycline treatment (3, 4). Several of these processes have been targeted therapeutically with little effect. For example, despite the well-characterized role of ROS overproduction in doxorubicin cardiotoxicity, clinical trials with the antioxidants

N-acetylcysteine and α-tocopherol did not show a cardioprotective effect in patients (5, 6), suggesting that ROS may not be the only inciting factor for doxorubicin cardiomyopathy.

Currently, dexrazoxane is the only Food and Drug Administration (FDA)–approved drug used clinically to prevent doxorubicin-induced heart failure. It is believed to chelate intracellular iron and block iron-assisted oxidative radical production (7, 8). Dexrazoxane may also protect cardiac cells by inhibiting topoisomerase IIβ, which has recently been implicated in the pathogenesis of doxorubicin cardiotoxicity (9, 10). However, in practice, the use of dexrazoxane is limited because of concerns that it may interfere with doxorubicin's ability to kill tumor cells (11). In addition, dexrazoxane has been reported to induce secondary malignancies (12), which has led to its removal from the market in Europe. As such, new approaches to cardioprotection are needed.

Zebrafish have been used successfully for high-throughput screening (HTS) to identify chemical compounds that suppress genetic defects and other disease states (13–15). Compared to cell-based in vitro systems, in vivo screening offers several advantages, including the ability to discover compounds with therapeutic activity even without knowing their molecular targets. In addition, compounds discovered by in vivo screening are selected for their ability to be effective in the complex context of the disease of interest. We therefore established a zebrafish model of doxorubicin-induced cardiomyopathy to screen for new cardioprotective compounds.

RESULTS

A doxorubicin-induced cardiomyopathy model in zebrafish

To avoid interference with early cardiogenesis, we started to treat zebrafish 1 day post-fertilization (dpf), after the heart had formed and circulation had begun. We treated animals with 100 μM doxorubicin and

[1]Cardiovascular Research Center, Massachusetts General Hospital and Harvard Medical School, Charlestown, MA 02129, USA. [2]Broad Institute, Cambridge, MA 02142, USA. [3]Department of Anesthesia, Critical Care and Pain Medicine, Massachusetts General Hospital and Harvard Medical School, Charlestown, MA 02129, USA. [4]Department of Pathology, Dalhousie University, Halifax, Nova Scotia B3H 4R2, Canada. [5]Massachusetts General Hospital Cancer Center and Harvard Medical School, Charlestown, MA 02129, USA. [6]Department of Biochemistry & Molecular Biology, Dalhousie University, Halifax, Nova Scotia B3H 4R2, Canada. [7]Martinos Center for Biomedical Imaging, Massachusetts General Hospital and Harvard Medical School, Charlestown, MA 02129, USA. [8]Howard Hughes Medical Institute. [9]Department of Pediatrics, Dalhousie University, Halifax, Nova Scotia B3H 4R2, Canada. [10]Department of Pediatrics, Izaak Walton Killam Health Centre, Halifax, Nova Scotia B3K 6R8, Canada.
*These authors contributed equally to this work.
†Corresponding author. E-mail: rtpeterson@mgh.harvard.edu

assessed phenotypic changes at 3 dpf (Fig. 1A). Two days after doxorubicin exposure, fish exhibited extensive pericardial edema. Microscopic examination revealed that the heart atrium was elongated and the ventricle collapsed (Fig. 1B). Heart contraction was markedly compromised, resulting in the absence of blood cell circulation within tail blood vessels (movies S1 and S2). Using a high-speed camera and a custom analysis algorithm (16), we calculated the fractional shortening of the zebrafish hearts. Both heart rate and contractility were markedly reduced in doxorubicin-treated fish (Fig. 1, C and F). We used a transgenic zebrafish line Tg(myl7:dsRed), which expresses the fluorescent protein dsRed from the myosin light chain promoter, to visualize individual cardiomyocytes. We found that both atrium and ventricle cardiomyocyte numbers were significantly reduced compared to controls (Fig. 1, D and G). TUNEL (terminal deoxynucleotidyl transferase–mediated deoxyuridine triphosphate nick end labeling) staining also showed that doxorubicin increased cardiomyocyte apoptosis (Fig. 1, E and H). Therefore, the zebrafish model recapitulated several aspects of doxorubicin-induced cardiomyopathy in humans, including increased apoptosis and reduced contractility. Because the doxorubicin-induced changes in cardiac function and blood circulation were easily detected visually, we used them as the basis of an assay to screen for small molecules that suppressed doxorubicin-induced cardiotoxicity.

Identification of compounds that prevent doxorubicin-induced cardiomyopathy in zebrafish

We screened 3000 small molecules from the Prestwick and Spectrum chemical libraries and identified eight compounds that could prevent doxorubicin-induced decreases in cardiac contraction and circulation. Two particularly potent agents, visnagin (VIS) and diphenylurea (DPU), were protective at concentrations less than 1 μM (Fig. 1, I and J). VIS, a furanochromone, and DPU, a urea derivative, belong to distinct structural classes. Three of the six less potent effective molecules shared clear structural similarity with VIS, confirming the efficacy of this structural class in preventing doxorubicin cardiotoxicity. VIS and DPU prevented the overt morphological effects of doxorubicin on the
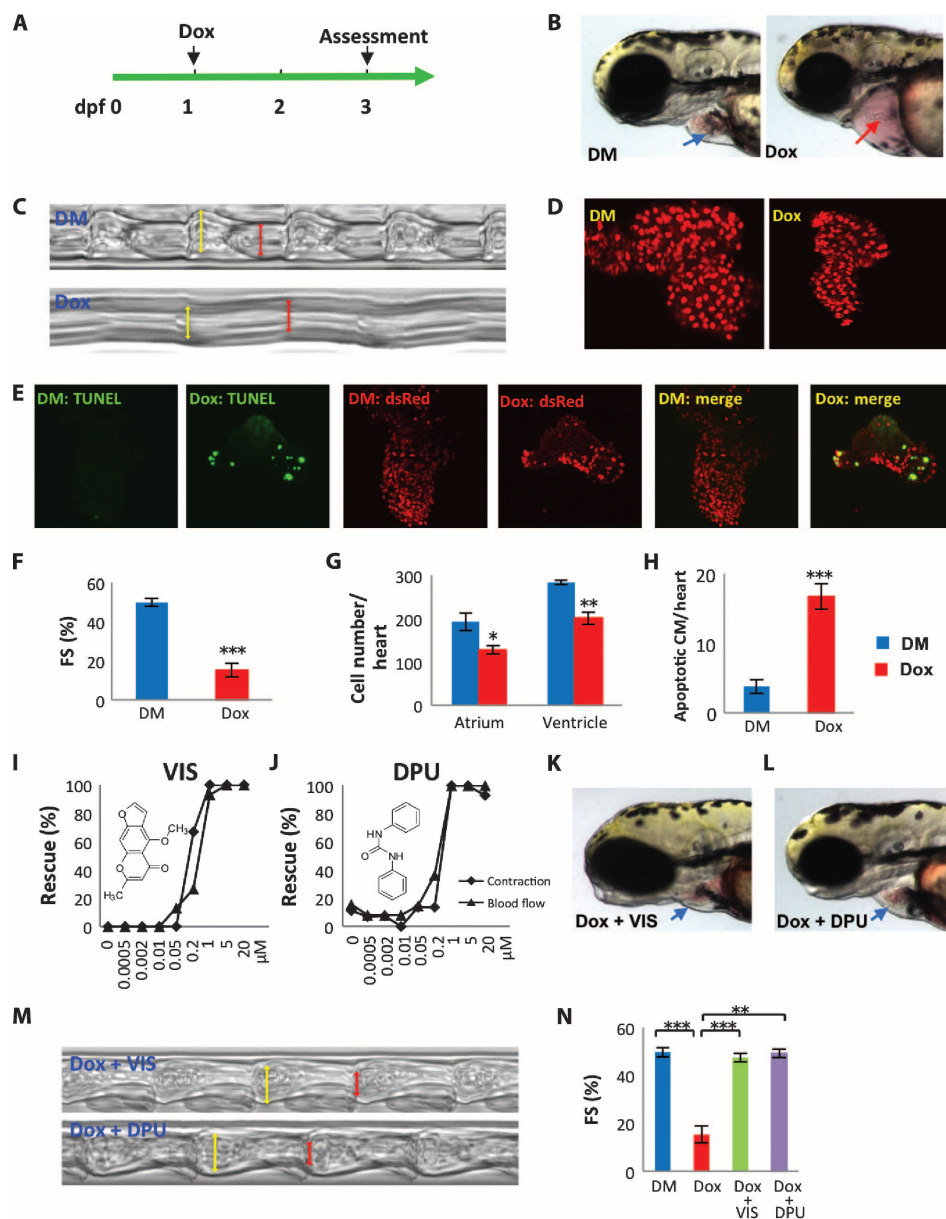
Fig. 1. Discovery of doxorubicin suppressors VIS and DPU in a doxorubicin-induced cardiomyopathy model in zebrafish. (**A**) Experimental scheme for inducing cardiomyopathy in zebrafish. Dox, doxorubicin. (**B**) Representative images of a normal heart (blue arrow) and doxorubicin-treated heart (red arrow). DM, DMSO (dimethyl sulfoxide) control. (**C** and **M**) Images reflecting heart contraction over time, derived from a region of interest drawn across the ventricle in sequential frames of high-speed video of the beating heart. (**D**) Representative images of cardiomyocytes genetically labeled with nuclear dsRed driven by a cardiomyocyte-specific myl7 promoter. (**E**) Detection of apoptotic cardiomyocytes by TUNEL staining. Green, TUNEL; red, cardiomyocytes; yellow, apoptotic cardiomyocytes. (**F**) Quantification of fractional shortening (FS) as follows: $(VID_d − VID_s)/VID_d × 100$. VID_d, diastolic ventricular internal dimension; VID_s, systolic ventricular internal dimension. n = 13 to 19 fish in each group, compared using Student's t test. (**G**) Quantification of cardiomyocyte number. n = 4 to 5 fish in each group, compared using Student's t test. (**H**) Quantification of apoptotic cardiomyocytes (CM). n = 4 to 5 fish in each group, compared using Student's t test. (**I** and **J**) VIS and DPU rescued heart contraction and blood flow in a dose-dependent manner, as manifested by the percentage of normal-looking fish out of total number of doxorubicin-treated fish. (**K** and **L**) Representative images showing grossly normal heart morphology in VIS or DPU rescued zebrafish. (**N**) Quantification of FS as follows: $(VID_d − VID_s)/VID_d × 100$. DM, DMSO-treated control samples; Dox, doxorubicin-treated samples; Dox + VIS, doxorubicin and VIS cotreated samples; Dox + DPU, doxorubicin and DPU cotreated samples. Statistics (compared to doxorubicin-treated samples): *$P < 0.05$, **$P < 0.01$, and ***$P < 0.001$.

heart, including ventricular collapse and pericardial edema (Fig. 1, K and L, and movie S3). Both compounds completely rescued cardiac contractility, as measured by fractional shortening (Fig. 1, M and N). VIS and DPU represent two distinct compound classes that potently protect the heart from the toxic effects of doxorubicin.

VIS and DPU effects on doxorubicin-induced cardiac cell death in vitro and in vivo

We determined whether VIS and DPU attenuated heart failure by inhibiting cardiomyocyte apoptosis. We first tested whether VIS and DPU attenuate doxorubicin-induced cell death of neonatal rat cardiomyocytes (NRCM) by TUNEL assay and annexin V staining. Both VIS and DPU significantly decreased doxorubicin-induced cell death (Fig. 2, A and B). Moreover, VIS and DPU also reduced doxorubicin-

induced cell death of a cardiac cell line HL1 (Fig. 2C) and consistently enhanced cell survival after doxorubicin treatment (Fig. 2D). Furthermore, we tested whether VIS and DPU inhibit cell death in doxorubicin-treated zebrafish and mice in vivo. In a transgenic zebrafish line expressing nuclear dsRed from the myl7 promoter in cardiomyocytes, we performed TUNEL staining to identify apoptotic cells after treatment with doxorubicin. Doxorubicin treatment caused a fourfold increase in apoptotic cardiomyocytes in zebrafish 4 dpf. VIS and DPU reduced the cardiomyocyte apoptotic index almost to baseline level (Fig. 2E).

To determine whether the ability of VIS and DPU to protect cardiomyocytes from apoptosis was conserved in mammals, we treated mice with doxorubicin with or without cotreatment with VIS or DPU. One day later, hearts were collected for apoptosis assays with TUNEL.
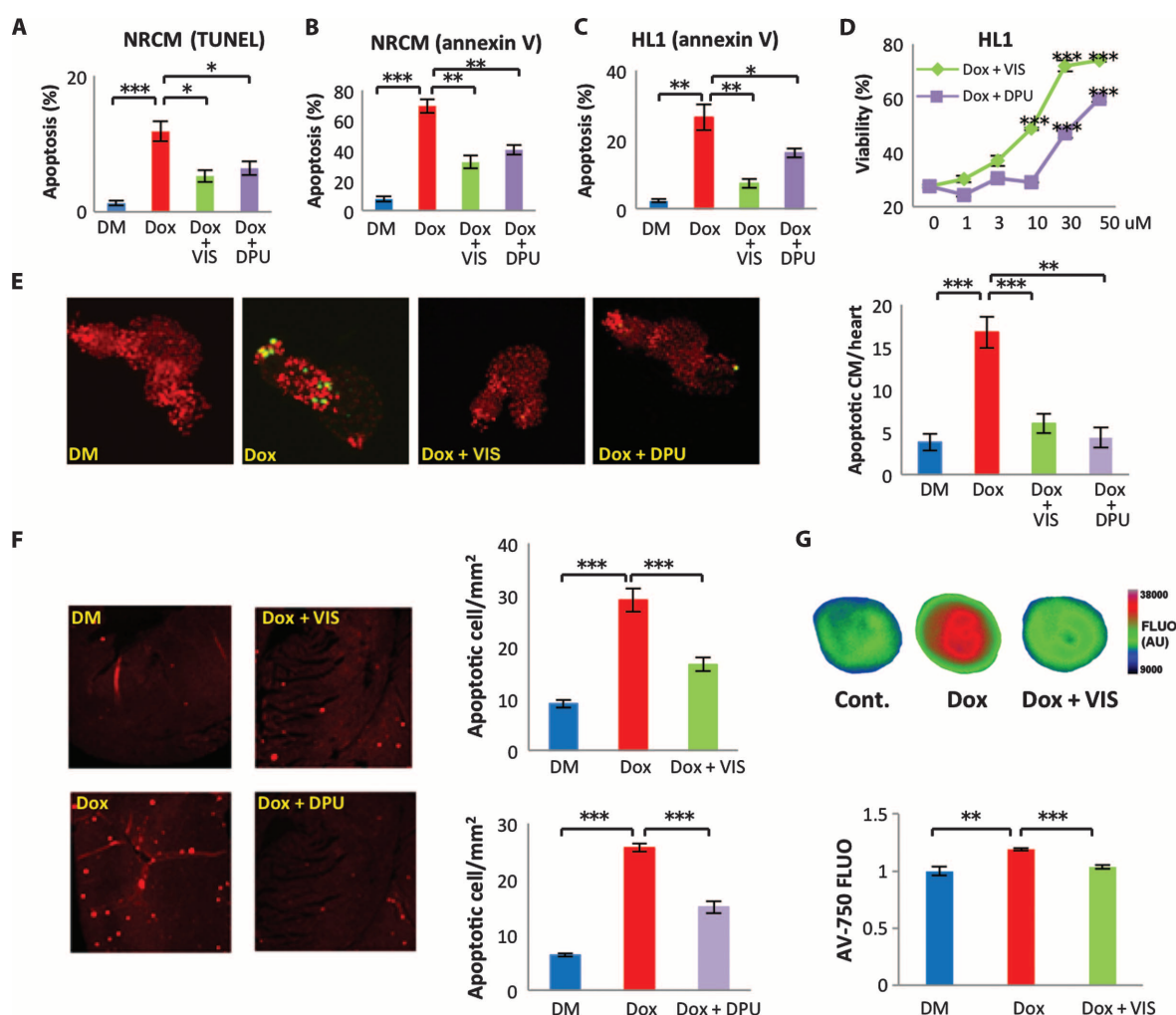
Fig. 2. VIS and DPU effects on doxorubicin-induced cardiac cell death in vitro and in vivo. (**A** and **B**) Doxorubicin-treated NRCM were treated with VIS and DPU and assessed for apoptosis with (A) TUNEL or (B) annexin V staining. (**C**) Doxorubicin-treated HL1 cells were treated with VIS or DPU and assessed for apoptosis with annexin V staining. (**D**) Viability of HL1 cells treated with doxorubicin and VIS or DPU. (**E** and **F**) Effect of VIS or DPU on cardiac cell death in doxorubicin-treated zebrafish (E) and mice (F) as measured by TUNEL assay. *n* = 3 to 9 zebrafish per group, or 4 to 5 mice per group. (**G**) Effect of VIS on doxorubicin-induced apoptosis in heart as assessed by ex vivo imaging of the whole heart with the dye AV-750. *n* = 5 mice per group, compared using one-way analysis of variance (ANOVA) and the Tukey posttest. DM, DMSO-treated control samples; Dox, doxorubicin-treated samples; Dox + VIS, doxorubicin and VIS cotreated samples; Dox + DPU, doxorubicin and DPU cotreated samples. Statistics (compared to doxorubicin-treated samples): *$P < 0.05$, **$P < 0.01$, and ***$P < 0.001$.

As seen in zebrafish, doxorubicin caused a three- to fourfold increase in apoptosis in mouse cardiac sections. Cotreatment with VIS or DPU significantly decreased doxorubicin-induced apoptosis (Fig. 2F). Furthermore, we tested the cardioprotective effect of VIS by ex vivo imaging with an annexin V conjugate with a near-infrared fluorochrome, Annexin-Vivo 750 (AV-750) (17). The result confirmed that VIS significantly reduced doxorubicin-induced apoptosis in mouse hearts (Fig. 2G). Therefore, VIS and DPU prevented doxorubicin-induced cardiac apoptosis in both zebrafish and mice.

Because published reports have implicated ROS production in the pathogenesis of doxorubicin cardiotoxicity, we tested hydrogen peroxide (H_2O_2) levels with CM-H2DCFDA staining in HL1 cultured cardiomyocytes. We observed an increase in H_2O_2 levels with doxorubicin treatment that was not affected by the addition of either VIS or DPU (fig. S1), suggesting that attenuation of H_2O_2-associated oxidative stress is not a key mechanism of cardioprotection with these agents.
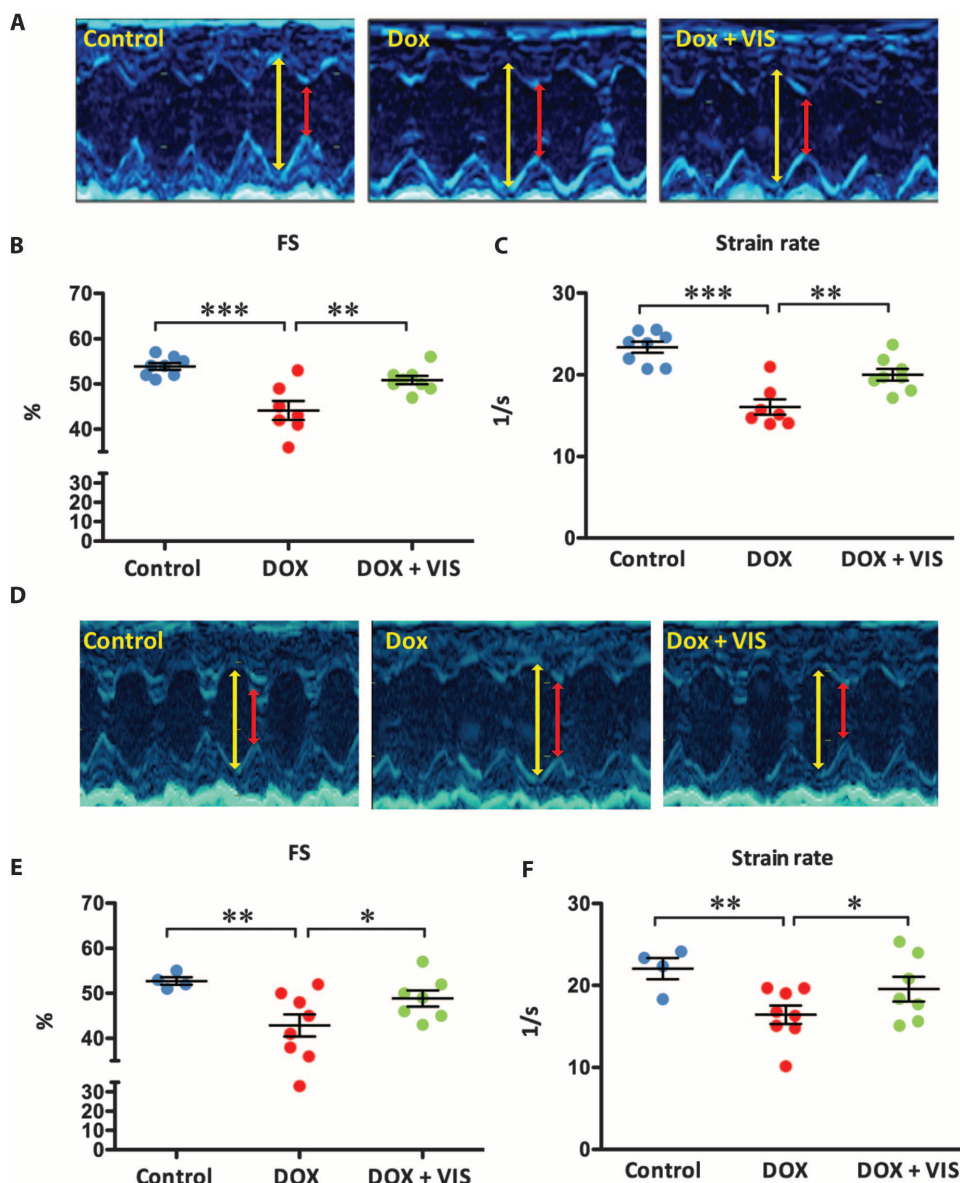
VIS effects on cardiac function in doxorubicin-treated mice

To determine whether the in vivo cardioprotective effect is conserved across species, we used two murine models of doxorubicin-induced cardiomyopathy. Because of the costs associated with testing two cardioprotectant compounds, we focused only on VIS for these studies. We induced acute cardiomyopathy by injecting mice with doxorubicin (15 mg/kg) intraperitoneally, and injected VIS (25 mg/kg) or vehicle immediately before doxorubicin injection. Five days after the initial injection, we assessed cardiac function by echocardiography and found that mice treated with doxorubicin and VIS exhibited significantly better fractional shortening and strain rate than did mice treated with doxorubicin alone (Fig. 3, A to C, and Table 1). Similarly, we induced cardiomyopathy by repeated injection of low-dosage doxorubicin for 5 weeks (5 mg/kg per week) followed by an additional 7 weeks without doxorubicin (18). VIS significantly improved cardiac function after doxorubicin treatment in this chronic model, as measured by fractional shortening and strain rate (Fig. 3, D to F, and Table 2).

VIS binding to MDH2

To identify the cardioprotective target of VIS, we performed a structure-activity relationship study of VIS and found that bergapten, a psoralen compound found in grapefruit juice, was a potent structural analog. We then synthesized a derivative of bergapten that had an alkyl linker capable of being attached to a solid support (Fig. 4A). Affinity chromatography of whole zebrafish lysates followed by silver staining revealed a single band that bound to bergapten-coupled beads. This binding was inhibited by free VIS (Fig. 4B). Mass spectrometry analysis identified the protein as mitochondrial malate dehydrogenase (MDH2). The specific binding of MDH2 to the affinity

Fig. 3. VIS effect on heart function in doxorubicin-treated mice. (**A** and **D**) Representative M-mode echocardiogram images of acute (A) and chronic (D) models: yellow line denotes left ventricular internal diameter at the end of diastole (LVIDd), and red line denotes left ventricular internal diameter at the end of systole (LVIDs). (**B**, **C**, **E**, and **F**) Effects of doxorubicin with and without VIS on fractional shortening (B and E) and strain rate (C and F) in both acute (B and C) and chronic (E and F) models. For acute models (B and C), groups were compared using one-way ANOVA followed by the Tukey posttest. For chronic models (E and F), groups were compared using one-way ANOVA followed by a one-tailed Student's *t* test. Control, vehicle-treated control mice; Dox, doxorubicin-treated mice; Dox + VIS, doxorubicin and VIS cotreated mice. Statistics (compared to doxorubicin-treated samples): *$P < 0.05$, **$P < 0.01$, and ***$P < 0.001$.

Table 1. Acute doxorubicin-induced cardiomyopathy mouse model.
Values are presented as means ± SEM. HR, heart rate; LVIDd, left ventricular internal diameter at the end of diastole; LVIDs, left ventricular internal diameter at the end of systole; FS, fractional shortening; Dox, doxorubicin. *$P <$ 0.05, **$P <$ 0.01, ***$P <$ 0.001, versus control. ‡$P <$ 0.05, ‡‡$P <$ 0.01, versus Dox.

	Control	Dox	Dox + VIS
HR (beats/min)	710 ± 15	605 ± 23**	640 ± 17*
LVIDd (mm)	3.22 ± 0.05	3.19 ± 0.09	3.08 ± 0.06
LVIDs (mm)	1.48 ± 0.04	1.78 ± 0.10*	1.51 ± 0.04‡
FS (%)	54 ± 1	44 ± 2***	51 ± 1‡‡
Strain rate (1/s)	23 ± 1	16 ± 1***	20 ± 1*‡‡
n	8	7	8

Table 2. Chronic doxorubicin-induced cardiomyopathy mouse model.
Values are presented as means ± SEM. Statistics (compared to control): *$P =$ 0.016 (LVIDs, Dox); **$P =$ 0.008 (HR, Dox), $P =$ 0.01 (FS, Dox), and $P =$ 0.006 (strain rate, Dox). Statistics (compared to Dox): ‡$P =$ 0.04 (FS, Dox + VIS) and $P =$ 0.05 (strain rate, Dox + VIS).

	Control	Dox	Dox + VIS
HR (beats/min)	752 ± 14	678 ± 14**	707 ± 21
LVIDd (mm)	3.26 ± 0.1	3.33 ± 0.04	3.42 ± 0.08
LVIDs (mm)	1.54 ± 0.07	1.91 ± 0.1*	1.76 ± 0.09
FS (%)	53 ± 1	43 ± 2**	49 ± 2‡
Strain rate (1/s)	22 ± 1	16 ± 1**	20 ± 2‡
n	4	8	7

beads was further confirmed by Western blotting with an anti-MDH2 antibody (Fig. 4C).

Effect of MDH2 inhibition and L-malic acid on doxorubicin cardiotoxicity

To determine whether MDH2 inhibition was responsible for the cardioprotective effect of VIS, structurally diverse MDH2 inhibitors were selected from the published literature and tested for their ability to protect the heart from doxorubicin (19, 20). In cultured HL1 cells, mebendazole, thyroxine (T4), and iodine all increased cardiomyocyte viability compared to doxorubicin treatment alone (Fig. 4D). Furthermore, cotreatment with any of these MDH2 inhibitors rescued zebrafish from doxorubicin-induced cardiotoxicity or death (Fig. 4E). Moreover, coadministration of L-malic acid protected the fish from development of the doxorubicin cardiotoxic phenotype in a dose-dependent fashion (Fig. 4F). Therefore, inhibition of MDH2 or exogenous augmentation of malate concentrations is sufficient to protect cardiac cells from doxorubicin toxicity.

Effects of inhibition of the malate-aspartate shuttle on doxorubicin cardiotoxicity

In addition to its role in the TCA (tricarboxylic acid) cycle, MDH2 is one of the key enzymes in the malate-aspartate shuttle (MAS). Because the inner mitochondrial membrane is impermeable to NADH (reduced form of nicotinamide adenine dinucleotide), the MAS is the primary mechanism by which electrons are transported across the mitochondrial membrane in the mammalian heart. To test the hypothesis that MDH2 inhibition confers its cardioprotective effects through inhibition of the MAS, we treated zebrafish embryos with doxorubicin and the MAS inhibitor aminooxyacetate (AOA). Coadministration of AOA protected fish from the development of doxorubicin cardiotoxicity in a dose-dependent manner (Fig. 4G) similarly to VIS, suggesting that VIS' cardioprotective effects may be related to MAS inhibition.

Effects of VIS and DPU on doxorubicin-induced tumor cell death in vitro or in vivo

The goal of the preceding studies was to identify compounds capable of reducing doxorubicin's cardiotoxicity but preserving its antitumor potency. Thus, we next determined whether VIS or DPU protects tumor cells from doxorubicin-mediated cell death. We tested whether VIS or

DPU at concentrations up to 50 μM protected several solid tumor lines from doxorubicin-induced cell death, including two prostate tumor lines, DU145 and LNCaP, and two breast cancer lines, MCF7 and MDA-MB-231. We found that VIS and DPU did not increase cell survival of any of the lines after doxorubicin treatment (Fig. 5, A to D).

We then determined whether VIS or DPU reduced the chemotherapeutic efficacy of doxorubicin in vivo. To this end, we used a zebrafish xenograft system in which Jurkat T-ALL leukemia cells were transplanted into zebrafish in vivo. We treated the recipient animals with doxorubicin with or without 20 μM VIS or DPU. Doxorubicin effectively reduced the burden of T-ALL cells in zebrafish. Cotreatment with VIS or DPU caused no reduction in doxorubicin's efficacy (Fig. 5E).

In addition, we tested VIS in a murine model in which MDA-MB-231 breast cancer cells had been transplanted into the mammary fat pad of NSG (NOD.Cg-Prkdc^scid Il2rg^tm1Wjl/SzJ) mice to generate xenograft tumors. Two weeks after initial cell implantation, mice were treated with vehicle, doxorubicin, or doxorubicin plus VIS, and the tumor size was assessed by caliper measurement throughout the experimental period from 0 to 20 days after treatment. Doxorubicin effectively reduced the mammary tumor burden in mice. VIS did not interfere with doxorubicin's efficacy (Fig. 5F), which was further confirmed by weighing tumors postmortem from different groups (Fig. 5, G and H). Together, these results indicate that VIS and DPU are effective cardioprotectants that do not interfere with doxorubicin's activity against a variety of cancer cell types.

DISCUSSION

With a doxorubicin-induced cardiomyopathy model in zebrafish, we conducted target-naïve, phenotype-based screening of a chemical library to identify newly described cardioprotective compounds. Two compounds, VIS and DPU, attenuate cardiac cell death and preserve cardiac function in zebrafish and mice. VIS and DPU do not interfere with doxorubicin-induced tumor cell death, underscoring the likelihood that the beneficial and detrimental effects of doxorubicin can be separated pharmacologically.

Neither VIS nor DPU has been previously linked to doxorubicin toxicity or heart failure. VIS is a natural product biosynthesized by the
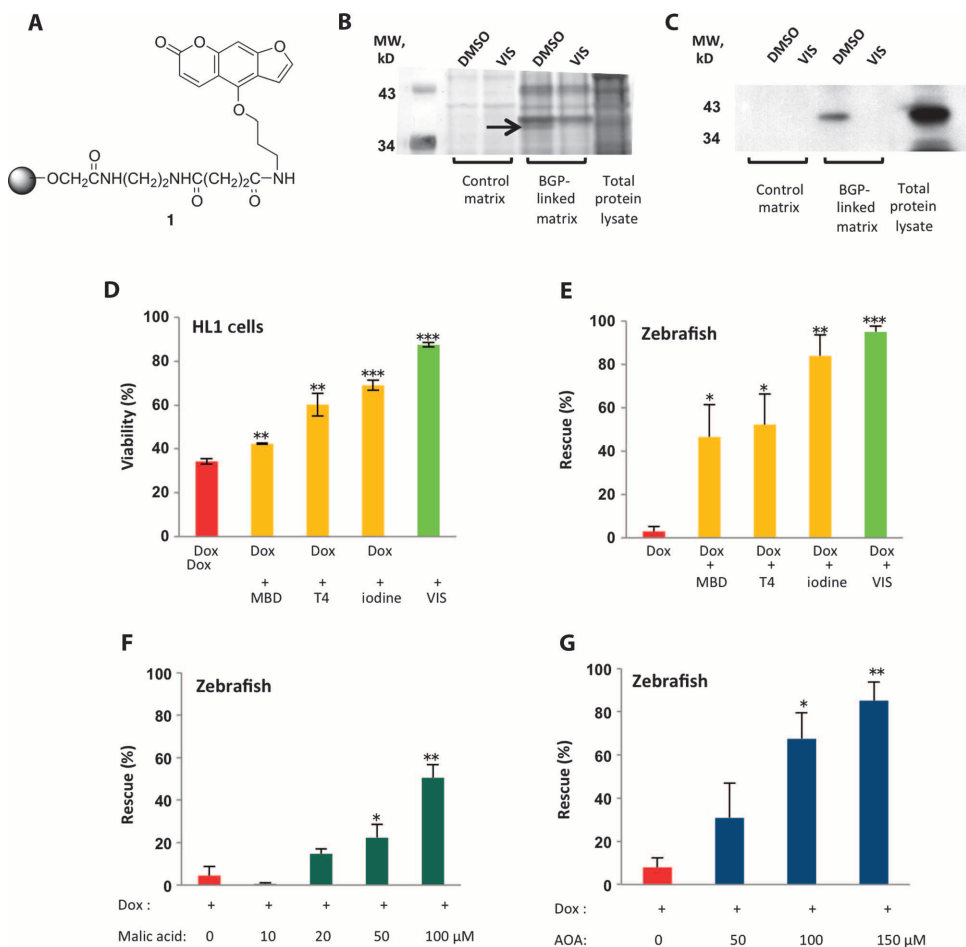
Fig. 4. VIS protects against doxorubicin cardiotoxicity through inhibition of MDH2. (**A**) Bergapten, a potent VIS derivative, with an alkyl linker that can be attached to a solid support (Compound **1**). (**B**) Electrophoresis gels of samples from affinity chromatography using a bergapten-linked matrix and competitive elution with VIS. BGP, bergapten; DM, DMSO. (**C**) Western blot of gel in (B) incubated with an anti-MDH2 antibody. (**D**) Viability measured in HL1 cardiomyocytes treated with doxorubicin and MDH2 inhibitors (MBD, 6.25 µM; T4, 100 µM; iodine, 200 µM). (**E**) Effect of MDH2 inhibitors on rescue from doxorubicin-induced cardiotoxicity and death in zebrafish. Rescue is calculated as the percentage of normal-appearing fish out of the total number of doxorubicin-treated fish (MBD, 1 µM; T4, 100 µM; iodine, 100 µM). MBD, mebendazole; T4, L-thyroxine. (**F**) Dose-dependent effects of L-malic acid on doxorubicin-induced cardiotoxicity and death. (**G**) Dose-dependent effects of the MAS inhibitor AOA on doxorubicin-induced cardiotoxicity and death. For (E) to (G), data were collected from a total of 150 zebrafish larvae treated for each condition, as measured over five independent experiments, and averaged. % Viability and % Rescue are depicted as mean ± SEM. *$P < 0.05$, **$P < 0.01$, and ***$P < 0.001$ using a two-tailed Student's t test.

and simultaneously attenuates doxorubicin cardiotoxicity in a rat breast cancer model, although MDH2 was not hypothesized as a mechanism (*25*). Similarly, heart-specific expression of human type 2 iodothyronine deiodinase in transgenic mice leads to elevated levels of thyroid hormone in the heart and better cardiac function after exposure to doxorubicin (*26*). Mebendazole has no known role in cardioprotection, but nonetheless rescued the cardiomyopathy phenotype in our zebrafish model. Iodine, thyroxine, and mebendazole are nonspecific compounds that modulate many targets, which may explain their reduced efficacy and increased toxicity relative to VIS. In summary, these structurally diverse MDH2 inhibitors mimic VIS' protective effects and suggest that MDH2 inhibition is sufficient to protect the heart from doxorubicin.

A major unanswered question is how MDH2 inhibition can be protective in cardiac cells without protecting cancer cells from doxorubicin. One possibility is that doxorubicin damages cardiac and cancer cells through different mechanisms, and that MDH2 inhibition interferes with the cardiac-specific mechanism. Although doxorubicin and the anthracyclines have been in clinical use for decades, it remains unclear how they induce cell death and whether they cause cell death through shared or distinct pathways in cardiac and cancer cells. Extensive studies have documented that doxorubicin triggers a number of cellular events including DNA damage and oxidative stress (*3*), and one or more of these processes may contribute to cell death in the heart more than in tumors. For example, VIS may modulate metabolic pathways that differentially contribute to the injury response in minimally proliferating cardiomyocytes and rapidly proliferating tumor cells, thereby preventing a maladaptive response to injury specifically in cardiomyocytes.

One intriguing possibility is the involvement of the MAS used to traffic reducing equivalents between mitochondria and the cytosol. Enzymes of the TCA cycle physically interact with MAS enzymes, allowing for direct communication of metabolic changes between the mitochondrial matrix and the cytosol (*27*). The TCA cycle is thought to function similarly in zebrafish and humans (*28*, *29*). Moreover, the amino acid sequences for the MAS enzymes MDH2 and aminoaspartate transferase share between 79 and 85% homology between zebrafish and humans, suggesting similar roles of these metabolic pathways across species (*30*). It has been proposed that MAS inhibition in cardiac cells decreases mitochondrial respiration before cardiac injury, thereby minimizing oxidative damage during recovery in a process that mimics
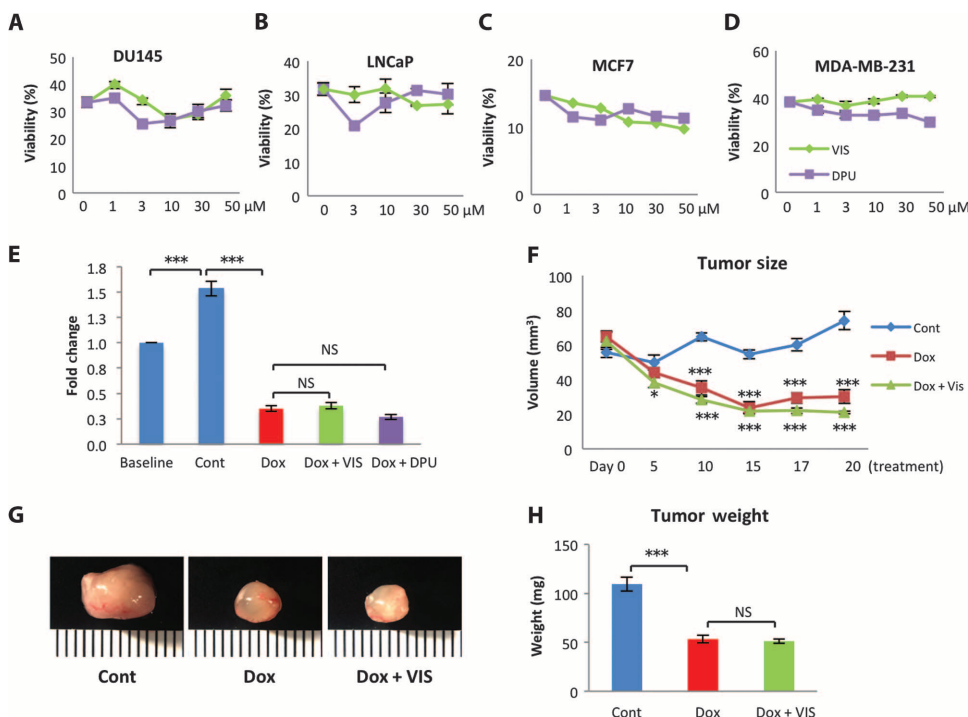
toothpick weed *Ammi visnaga* (*21*). Several previous papers have suggested a cell-protective effect for VIS. VIS can protect kidney epithelial cells from damage by oxalate and protect neurons from kainic acid–induced apoptosis (*22*, *23*). Furthermore, VIS inhibits lipopolysaccharide (LPS)–stimulated inflammation in a microglial cell line (*24*). Very little is known about the biological function and target of DPU.

Using an affinity chromatography approach, we discovered that VIS binds to MDH2. We observed cardioprotection with the administration of other MDH2 inhibitors, as well as with malic acid itself, suggesting that modulation of MDH2 may underlie VIS' therapeutic effect. For both iodine and thyroxine, hints of cardioprotection can be found in the literature. Iodine improves the antineoplastic effects of doxorubicin

Fig. 5. Lack of protective effect of VIS and DPU on doxorubicin-treated tumor cells in vitro and in vivo. (**A** to **D**) Effect of VIS or DPU on cell viability in multiple tumor lines including (A) DU145, (B) LNCaP, (C) MCF7, and (D) MDA-MB-231. (**E**) As measured by FACS (fluorescence-activated cell sorting) of dissociated tumor cells, change in size of xenografted human tumor derived from Jurkat cell injection in zebrafish in vivo treated with either 20 μM VIS or DPU. (**F**) Tumor volume of human tumor xenografts derived from injected MDA-MB-231 cells in mice treated with doxorubicin (2 mg/kg) and 20 VIS (mg/kg). Tumor size was assessed by caliper measurement of long axis a and short axis b, and was calculated with the following equation: $V = 1/2 \times a \times b^2$. $n = 8$ mice in each group. Statistics (compared to control samples): $*P = 0.04$ (day 5) and $***P = 8 \times 10^{-5}$ (Dox, day 10) and 1×10^{-8} (Dox + VIS, day 10); 3×10^{-5} (Dox, day 15) and 1×10^{-8} (Dox + VIS, day 15); 7×10^{-5} (Dox, day 17) and 1×10^{-7} (Dox + VIS, day 17); and 7×10^{-5} (Dox, day 20) and 8×10^{-8} (Dox + VIS, day 20). (**G**) Representative images of postmortem tumors from control, doxorubicin-treated, and doxorubicin plus VIS–treated mice. (**H**) Effect of VIS on doxorubicin-treated tumors. $***P = 2 \times 10^{-5}$ (compared to control samples). Cont, vehicle-treated control samples; Dox, doxorubicin-treated samples; Dox + VIS, doxorubicin plus VIS cotreated samples; Dox + DPU, doxorubicin plus DPU cotreated samples; NS, nonsignificant.

ischemic preconditioning (*31*). In contrast, tumor cells rely primarily on aerobic glycolysis rather than mitochondrial respiration via the well-characterized Warburg effect (*32*). Thus, it is conceivable that MAS inhibition may protect against a cardiotoxic injury without significantly affecting tumor metabolism and growth.

As with many animal studies, our study is limited by the challenges in translating findings in zebrafish and rodent models to the delayed-onset chronic cardiomyopathy seen in patients treated with doxorubicin. Before clinical use of the cardioprotective compounds identified in our screen, further experiments are needed to test different routes of administration, document any long-term toxicities, and confirm efficacy in preventing the development of cardiomyopathy. In addition, we tested a limited number of tumor cell lines and xenograft models, and it is unclear whether the preservation of doxorubicin's antitumor activity would extend to all types of malignancy. A more detailed characterization of the mechanisms behind MDH2-mediated cardioprotection may facilitate our understanding of the role of this pathway in cancer cell survival and growth.

Our data indicate that doxorubicin-induced cell death can be mitigated by VIS and DPU in a cell-specific fashion. Moreover, the discovery

that MDH2 inhibition is sufficient for cardioprotection provides a potential new therapeutic target and also a new entrance point for investigating the fundamental differences of responsiveness to doxorubicin by cardiac and tumor cells. Future experiments will focus on elucidating the role of MDH2 in doxorubicin's chemotherapeutic and cardiotoxic mechanisms. In addition, it will be informative to determine whether VIS' cardioprotective effects extend to other modes of cardiac injury, such as ischemia-reperfusion or other cardiotoxic chemotherapies.

MATERIALS AND METHODS

Study design
High-throughput chemical screening was performed in zebrafish embryos to identify novel therapies for doxorubicin-induced cardiotoxicity. Screen hits were confirmed in zebrafish embryos by measuring cardiomyocyte number, apoptosis, and fractional shortening; in male C57BL/6 mice by measuring TUNEL staining, annexin V whole-organ staining, and echocardiographic fractional shortening and strain rate; and in cultured HL1 cells by measuring cell viability and annexin V staining. The target of VIS was identified with affinity chromatography and mass spectrometry analysis followed by confirmatory Western blot. Finally, screen hits were tested in zebrafish and mouse xenograft tumor models, as well as in DU145, LNCaP, MCF7, and MDA-MB-231 tumor cell lines.

For mouse studies, sample size was selected on the basis of published data. Zebrafish cardiac function data and mouse echocardiographic data were analyzed by a study author blinded to the treatment conditions. All animals were randomly assigned to treatment groups for zebrafish cardiomyocyte counting, cardiac apoptosis, fractional shortening, and MDH2 inhibitor experiments, as well as for mouse cardiac apoptosis, annexin V staining, cardiac function assessment, and xenograft tumor experiments. Given the small size of these studies and similar genetic background of the animals in each group, no formal randomization protocol was used.

Animals
All zebrafish and mouse experiments were reviewed and approved by the Massachusetts General Hospital (MGH) Institutional Animal Care and Use Committee or the Dalhousie University Care of Laboratory Animals Committee.

Zebrafish model
Myl7-EGFP fish embryos (*33*) (1 dpf) were arrayed into 96-well plates, with each well containing three fish in 200 μl of E3 buffered with Hepes

(pH 7.2) with 100 µM doxorubicin. For screening, about 400 nl of small-molecule stock solution (in DMSO) was transferred from 96-well format library plates to the screening plates in the presence of iron [either using a stainless steel pin tool or through supplementation with ferric chloride (10 µM)]. At 3 dpf, treated fish were screened with an inverted fluorescence microscope (100×) for heart contraction and tail circulation.

Cell culture

NRCM were isolated from postnatal day 1 rats with a Neonatal Cardiomyocyte Isolation Kit (Worthington Biochemical) following the manufacturer's instruction, and cultured with L-15 medium.

Cardiac cell line HL1 was derived from mouse atrium tumor and was a gift from W. Claycomb. Culturing conditions were previously published (34). In brief, HL1 cells were cultured with Claycomb medium (Sigma) supplemented with fetal bovine serum (FBS), penicillin/streptomycin, L-glutamine, and norepinephrine.

DU145 and LNCaP are human prostate tumor lines, whereas MCF7 and MDA-MB-231 are human breast cancer lines. DU145, MCF7, and MDA-MB-231 cells were cultured with high-glucose Dulbecco's modified Eagle's medium (DMEM) (Life Sciences) supplemented with penicillin/streptomycin and L-glutamine, and LNCaP was grown in RPMI 1640 (Life Sciences) plus penicillin/streptomycin and L-glutamine.

Reagents

The Spectrum and Prestwick libraries were purchased from MicroSource Discovery Systems Inc. and Prestwick Chemical, respectively. Doxorubicin, VIS, DPU, mebendazole, L-thyroxine, iodine, L-malic acid, and amino-oxyacetic acid hemihydrochloride were obtained from Sigma-Aldrich. If not specified, all chemicals were dissolved in DMSO. The only exceptions were that doxorubicin was dissolved in saline and VIS was dissolved in vehicle containing 10% ethanol and 90% olive oil when injected into mice for the cardiac function and xenograft tumor studies.

Zebrafish cardiomyocyte counting

Myl7-nuc-dsRed fish (1 dpf) were treated with DMSO or 100 µM doxorubicin for 2 days (n = 5 each). Hearts were surgically removed and fixed with 4% paraformaldehyde (PFA) for 20 min at room temperature. The fixed heart samples were embedded in mounting medium and flattened with slide and coverslip. Confocal images were captured from the flattened hearts, and red nuclei were counted.

Zebrafish cardiac apoptosis assay

Myl7-nuc-dsRed fish larvae (1 dpf) were treated with DMSO, 100 µM doxorubicin, or doxorubicin plus 20 µM rescue compounds for 2 days (n = 5 each). Hearts were surgically removed and fixed with 4% PFA for 20 min at room temperature. After staining with an in situ TUNEL kit (Roche), heart samples were embedded in mounting medium, flattened with slide and coverslip, and then subjected to confocal microscopy. The data were quantified as percentage of TUNEL-positive cardiomyocytes.

Zebrafish heart fractional shortening measurement

Zebrafish (1 dpf) were treated with DMSO, doxorubicin, doxorubicin + VIS, or doxorubicin + DPU for 2 days (n = 13 to 19 each). High-speed video microscopy and measurement of ventricular size and function were performed as described (16). Briefly, M-mode images were assembled from sequential frames across a fixed scan line. Ventricular size was determined by measurement across endocardial borders at end systole and diastole, and fractional shortening was calculated.

Mouse cardiac apoptosis

Male C57BL/6 mice between 8 and 10 weeks were injected with DMSO, doxorubicin (15 mg/kg), or doxorubicin plus VIS (25 mg/kg) or DPU (10 mg/kg) intraperitoneally (n = 4 to 5 each). One day after injection, hearts were collected and fixed with 4% PFA at 4°C overnight, and then were subjected to paraffin embedding and sectioning. The heart sections were stained using the TMR TUNEL kit (Roche) following the manufacturer's protocol. The stained sections were scanned with MetaMorph-assisted slide scanning microscopy, and apoptosis indices were quantified as TUNEL-positive cell/mm^2.

Cell viability assay

Cultured HL1 and DU145 cells were treated with doxorubicin for the indicated amounts of time and were assayed using CellTiter-Glo Luminescent Cell Viability Assay (Promega).

Cell hydrogen peroxide (H_2O_2) detection

H_2O_2 production was assessed by CM-H2DCFDA (Invitrogen) staining as described (35). Briefly, cultured HL1 cells were treated with doxorubicin with or without VIS, DPU, or the general antioxidant scavenger 2-mercaptopropionyl-glycine (MPG) for 8 hours, and then stained with 10 mM CM-H2DCFDA and visualized by confocal microscopy (excitation/emission, 490/525 nm).

Annexin V staining

NRCM and HL1 cells were stained with fluorescent annexin V (Roche) and were live-imaged after being treated with doxorubicin for the indicated amounts of time. Apoptosis indices were quantified as percentage of annexin V–positive cells.

Whole-organ staining was performed with an annexin V conjugate with a near-infrared fluorochrome, AV-750 (PerkinElmer Life Sciences). Three cohorts of male C57BL/6 mice between 8 and 10 weeks of age (n = 5 each) were compared: untreated control, doxorubicin treatment, doxorubicin and VIS cotreatment. Twenty hours after treatment, mice were injected intravenously with 100 µl of AV-750. Four hours later, the mice were sacrificed according to the approved animal protocol, and the heart was imaged immediately in its short axis using a commercial imaging system (IVIS Spectrum, PerkinElmer). AV-750 fluorescence was detected with an excitation wavelength of 745 nm/emission wavelength of 800 nm, a 30-s exposure time, and a spatial resolution of 135 µm. Fluorescence standards of serially diluted AV-750 were imaged simultaneously, enabling calibration of the acquired signal. Total fluorescence within the left ventricle was quantified and normalized to the control mice.

Mouse cardiac function assessment

C57BL/6 male mice between 8 and 10 weeks of age were purchased from Charles River Laboratories and randomly grouped (n = 4 to 8). An acute heart failure model was generated by a single intraperitoneal injection of doxorubicin (15 mg/kg) dissolved in saline, whereas the chronic model involved intraperitoneal injection of doxorubicin (5 mg/kg) weekly for five consecutive weeks. In the treatment group, VIS (25 mg/kg) was dissolved in vehicle consisting of 10% ethanol and 90% olive oil, and then injected intraperitoneally and immediately

followed by contralateral doxorubicin injection. In the control group, plain vehicle and saline were injected instead. Five days (for the acute model) or 12 weeks (for the chronic model) after treatment, transthoracic echocardiographic images were obtained and interpreted by an echocardiographer blinded to the experimental design using a 13.0-MHz linear probe (Vivid 7, GE Medical System) as described (36, 37). Briefly, mice were lightly anesthetized with ketamine (20 mg/kg). M-mode images were obtained from a parasternal short-axis view at the midventricular level with a clear view of the papillary muscle. Tissue Doppler imaging was collected at a frame rate of 483 frames per second and a depth of 1 cm. LVIDd and LVIDs were measured. Fractional shortening was defined as [(LVIDd − LVIDs)/LVIDd] × 100. Strain rate of the posterior wall was analyzed offline in an EchoPAC workstation (GE Healthcare). In brief, a region of interest (axial distance, 0.2 mm; width, 0.6 mm) was manually positioned in the middle of the posterior wall. A strain length of 0.5 mm was used. Peak systolic strain rate was measured. The temporal smoothing filters were turned off for all measurements. The values of three consecutive cardiac cycles were averaged.

Procedure for immobilizing bergapten derivative to affinity chromatography matrix
Bergapten was identified as a potent structural analog of VIS. A bergapten derivative was synthesized via demethylation and alkylation of commercially available bergapten (Sigma-Aldrich) and coupled to Affi-Gel 10 affinity chromatography matrix.

Synthesis of 4-hydroxy-7H-furo[3,2-g]chromen-7-one 3: BBr$_3$ (8 ml, 8 mmol, 1 M in dichloromethane) was added dropwise to a solution of bergapten (432 mg, 2 mmol) in dichloromethane (8 ml), and the solution was stirred at 0°C for 2 hours. After completion of the reaction, saturated NaHCO$_3$ solution was poured slowly into the solution, resulting in the precipitation of a solid. The product was recovered by filtration, washed with cold water and ether, and dried under a high vacuum, yielding compound **3** as a white solid (303 mg, 1.50 mmol, 75%). ^{1}H NMR (500 MHz, d$_6$-DMSO) δ 11.35 (br, 1H), 8.23 (d, J = 9.5 Hz, 1H), 7.88 (d, J = 2.0 Hz, 1H), 7.17 (d, J = 2.5 Hz, 1H), 7.12 (s, 1H), 6.23 (d, J = 9.5 Hz, 1H); electrospray ionization mass spectrometry (ESI-MS) mass/charge ratio (m/z) 202 (M$^+$).


Synthesis of *tert*-butyl (3-((7-oxo-7H-furo[3,2-g]chromen-4-yl)oxy)propyl)carbamate 4: Compound **3** (40 mg, 0.2 mmol), 3-(Boc-amino)propyl bromide (48 mg, 0.2 mmol), and potassium carbonate (42 mg, 0.3 mmol) were mixed in dimethylformamide (DMF) (1 ml). The reaction mixture was heated under reflux until TLC (thin-layer chromatography) analysis (EA:Hex = 1:1, R_f = 0.4) confirmed that the reaction was complete. Water was added, and the mixture was extracted with ethyl acetate. The combined organic extracts were washed with saturated NaCl solution, dried over Na$_2$SO$_4$, and the solvent was removed in vacuo. The residue was purified via column chromatography, yield 90% (65 mg, 0.18 mmol). ^{1}H NMR (500 MHz, CDCl$_3$) δ 8.16 (d, J = 9.5 Hz, 1H), 7.59 (d, J = 4.5 Hz, 1H), 7.26 (d, J = 6.5 Hz, 1H), 7.15 (d, J = 6.5 Hz, 1H), 6.99

(s, 1H), 6.29 (d, J = 9.5 Hz, 1H), 4.52 (t, J = 6.0 Hz, 2H), 3.41 (t, J = 5.0 Hz, 2H,), 2.12 to 2.05 (m, 2H), 1.46 (s, 9H); ESI-MS m/z 359.7 (M$^+$).
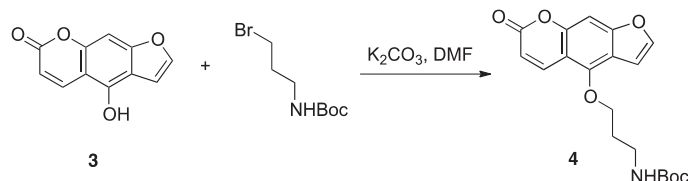
Synthesis of 4-(3-aminopropoxy)-7H-furo[3,2-g]chromen-7-one 5: To a stirring solution of compound **4** (36 mg, 0.1 mmol) in dry CH$_2$Cl$_2$ (1 ml) at 0°C, trifluoroacetic acid (0.1 ml) was slowly added, and the reaction mixture was stirred for 1 hour at room temperature. The mixture was concentrated under vacuum. The residue was suspended in ethyl acetate (10 ml), and a saturated NaHCO$_3$ solution was added to adjust the pH to 7 at 0 °C. The mixture was extracted with ethyl acetate (3 × 10 ml). The combined organic layer was dried over Na$_2$SO$_4$, filtered, and concentrated in vacuo. The crude product was used without further treatment, yield 95% (25 mg, 0.095 mmol). ^{1}H NMR (500 MHz, CDCl$_3$) δ 8.15 (d, J = 10.0 Hz, 1H), 7.59 (d, J = 2.0 Hz, 1H), 7.15 (s, 1H), 7.01 to 6.99 (m, 1H), 6.27 (d, J = 9.5 Hz, 1H), 6.29 (t, J = 9.5 Hz, 1H), 4.55 (t, J = 6.0 Hz, 2H), 2.99 (t, J = 7.0 Hz, 2H,), 2.04 to 2.00 (m, 2H); ESI-MS m/z 259.8 (M$^+$).
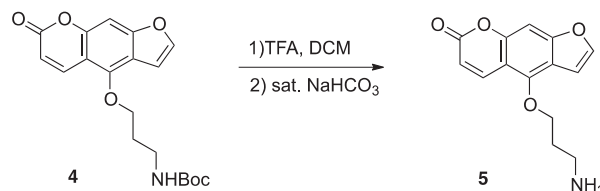
Coupling of bergapten derivative to immobilized agarose bead 1: Compound **4** (5 mg, 0.02 mmol), 1 ml of agarose beads (Affi-Gel 10; Bio-Rad, 0.015 mmol/ml) washed thoroughly with anhydrous DMSO, and *N,N*-diisopropylethylamine (6 μl, 0.03 mmol) were mixed in 1 ml of anhydrous DMSO. The mixture was rotated for 8 hours at room temperature. The resulting slurry was drained, and the beads were washed with water and DMSO. Bergapten-coupled agarose beads were stored in DMSO at 4°C.
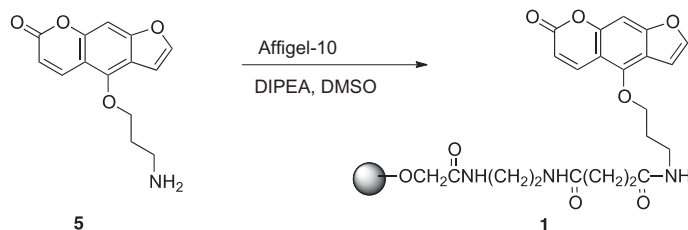
Affinity chromatography
Before chromatography, control and bergapten-coupled Affi-Gel matrix was blocked with bovine serum albumin (BSA) (2 mg/ml) and 1% goat serum overnight at 4°C. Sodium azide (0.2%) was added as an antimicrobial. Zebrafish larvae were homogenized in lysis buffer [10 mM tris (pH 7.4), 150 mM NaCl, 1 mM CaCl$_2$, 1% Triton X-100, supplemented with protease inhibitor cocktail and phosphatase inhibitor] at 72 hours post-fertilization (hpf) using a motorized pestle. The homogenate was

centrifuged for 10 min at 14,000g at 4°C. The supernatant was removed and diluted to a final protein concentration of 6 mg/ml. Control and bergapten-coupled matrix was suspended in phosphate-buffered saline (PBS) and incubated with the tissue lysate for 2 hours at 4°C. The supernatant was removed, and the matrix was washed four times with lysis buffer. The matrix was then incubated with VIS 500 µM (competitive elution) or an equivalent volume of DMSO (control elution) for 2 hours at 4°C. After removal of the supernatant, the matrix was serially washed with lysis buffer containing either VIS 500 µM or an equivalent volume of DMSO (half-hour incubation per wash). Protein bound to the matrix was denatured with sample buffer before gel electrophoresis. Total protein lysate was diluted 10-fold in lysis buffer and similarly denatured before gel electrophoresis.

Silver stain and mass spectrometry analysis

Equal quantities of protein were resolved on a 10% NuPAGE bis-tris gel. Silver staining was performed with a kit according to the manufacturer's protocol (Invitrogen). The band of interest was excised from the silver-stained gel and analyzed via liquid chromatography–tandem mass spectrometry (LC/MS-MS; Taplin Facility, Harvard Medical School). The excised gel band was cut into pieces and subjected to a modified in-gel trypsin digestion procedure (38) using a 50 mM ammonium bicarbonate solution containing modified sequencing-grade trypsin (12.5 ng/µl) (Promega) at 4°C. A nanoscale reversed-phase high-performance liquid chromatography capillary column was created as described (39). Each sample was loaded onto the column via a FAMOS autosampler (LC Packings). As peptides eluted, they were subjected to electrospray ionization and entered into an LTQ Orbitrap Velos Pro ion trap mass spectrometer (Thermo Fisher). Peptide sequences (and hence protein identity) were determined by matching protein databases with the acquired fragmentation pattern by the software program SEQUEST (Thermo Fisher) (40). Spectral matches were manually examined, and multiple identified peptides per protein were required.

Western blot confirmation of target identity

Affinity chromatography with competitive elution was performed as described. After SDS–polyacrylamide gel electrophoresis, proteins were transferred to a polyvinylidene difluoride membrane (Bio-Rad), blocked with 5% BSA, and incubated with anti-MDH2 antibody (Sigma-Aldrich) at 4°C overnight. Immunodetection was performed with a mouse anti-rabbit immunoglobulin G (IgG) light chain–specific secondary antibody (Jackson ImmunoResearch) and Amersham ECL Prime Western Blotting Detection Reagent (GE Healthcare Life Sciences).

MDH2 inhibitor, L-malic acid, and AOA treatment

HL1 cardiomyocytes and Tübingen AB (TuAB) zebrafish embryos at 30 hpf were treated with doxorubicin (100 µM) and one of several MDH2 inhibitors, L-malic acid, or AOA. The highest nontoxic dose was chosen for each MDH2 inhibitor (mebendazole: 6.25 µM in cultured cells and 1 µM in zebrafish; thyroxine: 100 µM in both cultured cells and zebrafish; iodine: 200 µM in cultured cells and 100 µM in zebrafish). One hundred fifty zebrafish embryos were treated for each condition. Assessment of phenotype was performed 28 hours after treatment in cultured cells and 48 hours after treatment in zebrafish.

Xenograft tumor models

Mouse. Six-week-old female NSG (NOD.Cg-Prkdcscid Il2rgtm1Wjl/SzJ) mice (Jackson Laboratory) were anesthetized with isoflurane. MDA-MB-231 cells (1×10^6) in 100 µl of 1:1 PBS and Matrigel (BD Biosciences) were injected into the fourth right mammary fat pad. Two weeks after tumor cell implantation, mice were randomly grouped ($n = 8$ each) and treated once a week for 2 weeks (days 0 and 7) with vehicle, doxorubicin (2 mg/kg body weight), or doxorubicin (2 mg/kg body weight) + VIS (20 mg/kg body weight).

Zebrafish. Mutant *casper* zebrafish embryos (41) at 24 hpf were anesthetized with tricaine (0.090 mg/ml) (Sigma-Aldrich) and used for cell transplantation using a protocol adapted from (42, 43). Briefly, CM-Dil–labeled leukemia cells were loaded into a pulled glass micropipette, and about 50 cells were delivered, as a single injection, into the yolk sac of each embryo using a PLI-100A Pico-Liter Injector (Warner instruments). After injection, embryos were allowed to recover at 28°C for 1 hour before transfer to 35°C, where they remained for the experiment.

At 4 hours after injection, only embryos with a uniform fluorescent cell mass at the site of injection were randomized and divided into four groups ($n = 15$ to 20) for proliferation studies. Embryos xenotransplanted with human cancer cells were then treated with 100 µM doxorubicin and 20 µM VIS or DPU, and embryos were incubated for 48 hours until 72 hpf. Embryos treated with vehicle (0.1% DMSO) served as a negative control for drug efficacy (43).

For the fluorescence imaging, a filter with excitation/emission wavelengths of 550/605 nm was used, and all embryos were photographed under the same settings. Groups of 15 to 20 xenografted embryos were dissociated into a single-cell suspension, and leukemia cells were enumerated by counting cells positive for PML bodies (found in human cells but not in zebrafish cells). This was accomplished by performing cytospin (cytospin conditions: 300 rpm for 10 min, using a Shandon CytoSpin 3, Global Medical Instrumentation) of dissociated embryos, and immunohistochemistry for PML bodies [primary antibody: rabbit anti-PML (Santa Cruz, sc-5621); secondary antibody: DyLight donkey anti-rabbit IgG 649 (Abcam)]. Fluorescent images were acquired on a custom-built Zeiss Axio Observer Z1 inverted microscope equipped with 405-, 488-, 561-, and 633-nm diode-based lasers [Intelligent Imaging Innovations (3i)] and a confocal spinning disc unit (CSU-X1) (Yokogawa). Cells were observed using a 10× objective, and images were recorded using an Evolve 512 electron-multiplying charge-coupled device (EMCCD) camera (Photometrics) and SlideBook 5.1 software using the mosaic tool [Intelligent Imaging Innovations (3i)]. The experiments were done three independent times.

Statistical analysis

For zebrafish cardiomyocyte counting, cell viability assay, and zebrafish and mouse cardiac apoptosis assays, experiments were performed at least three times, and statistics were obtained by Student's t test. For the ex vivo annexin V apoptosis assay, annexin uptake was compared among the three groups of mice (control versus Dox versus Dox + VIS) with one-way ANOVA and the Tukey posttest. Echo data were analyzed by one-way ANOVA with the Tukey posttest for the acute model or one-tailed t test for the chronic model. Treatment with MDH2 inhibitors and L-malic acid in zebrafish was performed over five independent experiments and analyzed with two-tailed Student's t test.

SUPPLEMENTARY MATERIALS

www.sciencetranslationalmedicine.org/cgi/content/full/6/266/266ra170/DC1
Fig. S1. VIS and DPU do not decrease ROS levels.
Movie S1. (DMSO.m4v): Heart contraction of 3-dpf zebrafish treated with vehicle (1% DMSO in E3 water).
Movie S2. (DOX.m4v): Heart contraction of 3-dpf zebrafish treated with 100 µM Dox.
Movie S3. (DOX + VIS.m4v): Heart contraction of 3-dpf zebrafish cotreated with Dox (100 µM) and VIS (20 µM).

REFERENCES AND NOTES

1. T. M. Suter, M. S. Ewer, Cancer drugs and the heart: Importance and management. *Eur. Heart J.* **34**, 1102–1111 (2013).

2. S. E. Lipshultz, T. R. Cochran, V. I. Franco, T. L. Miller, Treatment-related cardiotoxicity in survivors of childhood cancer. *Nat. Rev. Clin. Oncol.* **10**, 697–710 (2013).

3. B. Ky, P. Vejpongsa, E. T. Yeh, T. Force, J. J. Moslehi, Emerging paradigms in cardiomyopathies associated with cancer therapies. *Circ. Res.* **113**, 754–764 (2013).

4. Y. Octavia, C. G. Tocchetti, K. L. Gabrielson, S. Janssens, H. J. Crijns, A. L. Moens, Doxorubicin-induced cardiomyopathy: From molecular mechanisms to therapeutic strategies. *J. Mol. Cell. Cardiol.* **52**, 1213–1225 (2012).

5. C. Myers, R. Bonow, S. Palmeri, J. Jenkins, B. Corden, G. Locker, J. Doroshow, S. Epstein, A randomized controlled trial assessing the prevention of doxorubicin cardiomyopathy by N-acetylcysteine. *Semin. Oncol.* **10**, 53–55 (1983).

6. S. S. Legha, Y. M. Wang, B. Mackay, M. Ewer, G. N. Hortobagyi, R. S. Benjamin, M. K. Ali, Clinical and pharmacologic investigation of the effects of a-tocopherol on adriamycin cardiotoxicity. *Ann. N.Y. Acad. Sci.* **393**, 411–418 (1982).

7. B. B. Hasinoff, E. H. Herman, Dexrazoxane: How it works in cardiac and tumor cells. Is it a prodrug or is it a drug. *Cardiovasc. Toxicol.* **7**, 140–144 (2007).

8. Y. Ichikawa, M. Ghanefar, M. Bayeva, R. Wu, A. Khechaduri, S. V. Naga Prasad, R. K. Mutharasan, T. J. Naik, H. Ardehali, Cardiotoxicity of doxorubicin is mediated through mitochondrial iron accumulation. *J. Clin. Invest.* **124**, 617–630 (2014).

9. Y. L. Lyu, J. E. Kerrigan, C. P. Lin, A. M. Azarova, Y. C. Tsai, Y. Ban, L. F. Liu, Topoisomerase IIβ–mediated DNA double-strand breaks: Implications in doxorubicin cardiotoxicity and prevention by dexrazoxane. *Cancer Res.* **67**, 8839–8846 (2007).

10. S. Zhang, X. Liu, T. Bawa-Khalfe, L. S. Lu, Y. L. Lyu, L. F. Liu, E. T. Yeh, Identification of the molecular basis of doxorubicin-induced cardiotoxicity. *Nat. Med.* **18**, 1639–1642 (2012).

11. S. M. Swain, F. S. Whaley, M. C. Gerber, S. Weisberg, M. York, D. Spicer, S. E. Jones, S. Wadler, A. Desai, C. Vogel, J. Speyer, A. Mittelman, S. Reddy, K. Pendergrass, E. Velez-Garcia, M. S. Ewer, J. R. Bianchine, R. A. Gams, Cardioprotection with dexrazoxane for doxorubicin-containing therapy in advanced breast cancer. *J. Clin. Oncol.* **15**, 1318–1332 (1997).

12. C. K. Tebbi, W. B. London, D. Friedman, D. Villaluna, P. A. De Alarcon, L. S. Constine, N. P. Mendenhall, R. Sposto, A. Chauvenet, C. L. Schwartz, Dexrazoxane-associated risk for acute myeloid leukemia/myelodysplastic syndrome and other secondary malignancies in pediatric Hodgkin's disease. *J. Clin. Oncol.* **25**, 493–500 (2007).

13. X. Le, E. K. Pugach, S. Hettmer, N. Y. Storer, J. Liu, A. A. Wills, A. DiBiase, E. Y. Chen, M. S. Ignatius, K. D. Poss, A. J. Wagers, D. M. Langenau, L. I. Zon, A novel chemical screening strategy in zebrafish identifies common pathways in embryogenesis and rhabdomyosarcoma development. *Development* **140**, 2354–2364 (2013).

14. R. M. White, J. Cech, S. Ratanasirintrawoot, C. Y. Lin, P. B. Rahl, C. J. Burke, E. Langdon, M. L. Tomlinson, J. Mosher, C. Kaufman, F. Chen, H. K. Long, M. Kramer, S. Datta, D. Neuberg, S. Granter, R. A. Young, S. Morrison, G. N. Wheeler, L. I. Zon, DHODH modulates transcriptional elongation in the neural crest and melanoma. *Nature* **471**, 518–522 (2011).

15. R. T. Peterson, S. Y. Shaw, T. A. Peterson, D. J. Milan, T. P. Zhong, S. L. Schreiber, C. A. MacRae, M. C. Fishman, Chemical suppression of a genetic mutation in a zebrafish model of aortic coarctation. *Nat. Biotechnol.* **22**, 595–599 (2004).

16. J. T. Shin, E. V. Pomerantsev, J. D. Mably, C. A. MacRae, High-resolution cardiovascular function confirms functional orthology of myocardial contractility pathways in zebrafish. *Physiol. Genomics* **42**, 300–309 (2010).

17. H. H. Chen, L. Josephson, D. E. Sosnovik, Imaging of apoptosis in the heart with nanoparticle technology. *Wiley Interdiscip. Rev. Nanomed. Nanobiotechnol.* **3**, 86–99 (2011).

18. A. Hiona, A. S. Lee, J. Nagendran, X. Xie, A. J. Connolly, R. C. Robbins, J. C. Wu, Pretreatment with angiotensin-converting enzyme inhibitor improves doxorubicin-induced cardiomyopathy via preservation of mitochondrial function. *J. Thorac. Cardiovasc. Surg.* **142**, 396–403.e3 (2011).

19. S. Varrone, E. Consiglio, I. Covelli, The nature of inhibition of mitochondrial malate dehydrogenase by thyroxine, iodine cyanide and molecular iodine. *Eur. J. Biochem.* **13**, 305–312 (1970).

20. P. Tejada, M. Sanchez-Moreno, M. Monteoliva, H. Gomez-Banqueri, Inhibition of malate dehydrogenase enzymes by benzimidazole anthelmintics. *Vet. Parasitol.* **24**, 269–274 (1987).

21. B. Kaul, E. J. Staba, Visnagin: Biosynthesis and isolation from Ammi visnaga suspension cultures. *Science* **150**, 1731–1732 (1965).

22. P. Vanachayangkul, K. Byer, S. Khan, V. Butterweck, An aqueous extract of *Ammi visnaga* fruits and its constituents khellin and visnagin prevent cell damage caused by oxalate in renal epithelial cells. *Phytomedicine* **17**, 653–658 (2010).

23. M. S. Kwon, J. K. Lee, S. H. Park, Y. B. Sim, J. S. Jung, M. H. Won, S. M. Kim, H. W. Suh, Neuroprotective effect of visnagin on kainic acid-induced neuronal cell death in the mice hippocampus. *Korean J. Physiol. Pharmacol.* **14**, 257–263 (2010).

24. J. K. Lee, J. S. Jung, S. H. Park, S. H. Park, Y. B. Sim, S. M. Kim, T. S. Ha, H. W. Suh, Anti-inflammatory effect of visnagin in lipopolysaccharide-stimulated BV-2 microglial cells. *Arch. Pharm. Res.* **33**, 1843–1850 (2010).

25. Y. Alfaro, G. Delgado, A. Cárabez, B. Anguiano, C. Aceves, Iodine and doxorubicin, a good combination for mammary cancer treatment: Antineoplastic adjuvancy, chemoresistance inhibition, and cardioprotection. *Mol. Cancer* **12**, 45 (2013).

26. E. G. Hong, B. W. Kim, D. Y. Jung, J. H. Kim, T. Yu, W. Seixas Da Silva, R. H. Friedline, S. D. Bianco, S. P. Seslar, H. Wakimoto, C. I. Berul, K. S. Russell, K. W. Lee, P. R. Larsen, A. C. Bianco, J. K. Kim, Cardiac expression of human type 2 iodothyronine deiodinase increases glucose metabolism and protects against doxorubicin-induced cardiac dysfunction in male mice. *Endocrinology* **154**, 3937–3946 (2013).

27. S. Beeckmans, L. Kanarek, Demonstration of physical interactions between consecutive enzymes of the citric acid cycle and of the aspartate-malate shuttle. A study involving fumarase, malate dehydrogenase, citrate synthesis and aspartate aminotransferase. *Eur. J. Biochem.* **117**, 527–535 (1981).

28. M. Kanehisa, S. Goto, KEGG: Kyoto encyclopedia of genes and genomes. *Nucleic Acids Res.* **28**, 27–30 (2000).

29. M. Kanehisa, S. Goto, Y. Sato, M. Kawashima, M. Furumichi, M. Tanabe, Data, information, knowledge and principle: Back to metabolism in KEGG. *Nucleic Acids Res.* **42**, D199–D205 (2014).

30. S. F. Altschul, T. L. Madden, A. A. Schaffer, J. Zhang, Z. Zhang, W. Miller, D. J. Lipman, Gapped BLAST and PSI-BLAST: A new generation of protein database search programs. *Nucleic Acids Res.* **25**, 3389–3402 (1997).

31. T. T. Nielsen, N. B. Støttrup, B. Løfgren, H. E. Bøtker, Metabolic fingerprint of ischaemic cardioprotection: Importance of the malate–aspartate shuttle. *Cardiovasc. Res.* **91**, 382–391 (2011).

32. O. Warburg, On respiratory impairment in cancer cells. *Science* **124**, 269–270 (1956).

33. W. Rottbauer, G. Wessels, T. Dahme, S. Just, N. Trano, D. Hassel, C. G. Burns, H. A. Katus, M. C. Fishman, Cardiac myosin light chain-2: A novel essential component of thick-myofilament assembly and contractility of the heart. *Circ. Res.* **99**, 323–331 (2006).

34. W. C. Claycomb, N. A. Lanson Jr., B. S. Stallworth, D. B. Egeland, J. B. Delcarpio, A. Bahinski, N. J. Izzo Jr., HL-1 cells: A cardiac muscle cell line that contracts and retains phenotypic characteristics of the adult cardiomyocyte. *Proc. Natl. Acad. Sci. U.S.A.* **95**, 2979–2984 (1998).

35. P. Korge, P. Ping, J. N. Weiss, Reactive oxygen species production in energized cardiac mitochondria during hypoxia/reoxygenation: Modulation by nitric oxide. *Circ. Res.* **103**, 873–880 (2008).

36. L. Zou, Y. Feng, Y. J. Chen, R. Si, S. Shen, Q. Zhou, F. Ichinose, M. Scherrer-Crosbie, W. Chao, Toll-like receptor 2 plays a critical role in cardiac dysfunction during polymicrobial sepsis. *Crit. Care Med.* **38**, 1335–1342 (2010).

37. T. G. Neilan, D. S. Jassal, T. M. Perez-Sanz, M. J. Raher, A. D. Pradhan, E. S. Buys, F. Ichinose, D. B. Bayne, E. F. Halpern, A. E. Weyman, G. Derumeaux, K. D. Bloch, M. H. Picard, M. Scherrer-Crosbie, Tissue Doppler imaging predicts left ventricular dysfunction and mortality in a murine model of cardiac injury. *Eur. Heart J.* **27**, 1868–1875 (2006).

38. A. Shevchenko, M. Wilm, O. Vorm, M. Mann, Mass spectrometric sequencing of proteins silver-stained polyacrylamide gels. *Anal. Chem.* **68**, 850–858 (1996).

39. J. Peng, S. P. Gygi, Proteomics: The move to mixtures. *J. Mass Spectrom.* **36**, 1083–1091 (2001).

40. J. K. Eng, A. L. McCormack, J. R. Yates, An approach to correlate tandem mass spectral data of peptides with amino acid sequences in a protein database. *J. Am. Soc. Mass Spectrom.* **5**, 976–989 (1994).

41. R. M. White, A. Sessa, C. Burke, T. Bowman, J. LeBlanc, C. Ceol, C. Bourque, M. Dovey, W. Goessling, C. E. Burns, L. I. Zon, Transparent adult zebrafish as a tool for in vivo transplantation analysis. *Cell Stem Cell* **2**, 183–189 (2008).

42. M. Haldi, C. Ton, W. L. Seng, P. McGrath, Human melanoma cells transplanted into zebrafish proliferate, migrate, produce melanin, form masses and stimulate angiogenesis in zebrafish. *Angiogenesis* **9**, 139–151 (2006).

43. D. P. Corkery, G. Dellaire, J. N. Berman, Leukaemia xenotransplantation in zebrafish—Chemotherapy response assay in vivo. *Br. J. Haematol.* **153**, 786–789 (2011).

Editor's Summary

Taming the Red Devil

The cancer chemotherapy drug doxorubicin saves lives but its propensity to also inflict damage on the heart has earned it the nickname of the Red Devil. Liu *et al.* have now identified a compound that can prevent this drug-induced heart damage while leaving its cancer killing qualities intact. This agent, visnatin, was found among 3000 tested on a versatile piscine model, the zebrafish. After doxorubicin treatment, zebrafish hearts too suffer damage and visnagin protected them from injury. These salutary effects of visnagin were also apparent in mice, where it acts through mitochondrial malate dehydrogenase, a key metabolic enzyme. This or similar drugs may prove to be a valuable companion for doxorubicin, allowing it to acquire a less fiendish nickname.